Chemical Engineering Journal 231 (2013) 198–205

Contents lists available at SciVerse ScienceDirect

Chemical Engineering Journal

journal homepage: www.elsevier.com/locate/cej

Excellent fluoride removal performance by CeO_2–ZrO_2 nanocages in water environment

Jing Wang [a,b], Weihong Xu [a,b,*], Liang Chen [a,b], Yong Jia [b], Lei Wang [a,b], Xing-Jiu Huang [a,b,*], Jinhuai Liu [a,b]

[a] Department of Materials Science and Engineering, University of Science and Technology of China, Hefei, Anhui 230026, PR China
[b] Nano-Materials and Environmental Detection Laboratory, Hefei Institute of Intelligent Machines, Chinese Academy of Sciences, Hefei, Anhui 230031, PR China

HIGHLIGHTS

- CeO_2–ZrO_2 nanocages with high capacity and affinity for fluoride were prepared.
- The adsorbent kept good adsorption capacity for fluoride around pH 3.0–7.0.
- The adsorption mechanisms involved anion exchange and electrostatic interaction.

ARTICLE INFO

Article history:
Received 29 April 2013
Received in revised form 6 July 2013
Accepted 8 July 2013
Available online 17 July 2013

Keywords:
Fluoride
CeO_2–ZrO_2 nanocages
Adsorption
Drinking water

ABSTRACT

CeO_2–ZrO_2 nanocages were prepared by Kirkendall effect, and their fluoride removal performance was investigated in batch studies. The obtained CeO_2–ZrO_2 adsorbent presented a good adsorption capacity in the pH range of 3.0–7.0, and the optimum pH range was 3.5–4.5. The adsorption isotherm could be better described by the Langmuir model than the Freundlich model. The Langmuir maximum capacity of the CeO_2–ZrO_2 adsorbent was calculated to be 175 mg/g at pH 4.0, which was much higher than that of other adsorbents reported previously. The effect of co-existing anions, such as sulfate, chloride, arsenate, and bicarbonate, on fluoride adsorption was systematically studied. Furthermore, the as-prepared adsorbent showed an excellent fluoride removal properties in real underground water. The adsorption mechanism was investigated by zeta potential measurement, Fourier transform infrared (FTIR), and X-ray photoelectron spectroscopy (XPS) analysis. Anion exchange and electrostatic interaction play key roles in fluoride removal.

1. Introduction

Fluoride contamination of groundwater through a combination of natural processes and anthropogenic activities is a major problem worldwide [1,2]. It has been reported that more than 200 million people worldwide regularly take fluoride contaminated water for drinking that exceeds the present WHO guideline of 1.5 mg/L [3,4]. Excess intake of fluoride can cause harmful effects such as dental/skeletal fluorosis, fetal cerebral function, and neurotransmitters [1,4]. Considering the serious health effects, several technologies, including precipitation, adsorption, ion exchange, membrane separation and electrodialysis, have been developed for fluoride removal. Among these methods, adsorption seems to be a more attractive method for the removal of fluoride in terms of cost, simplicity of design and operation. Various adsorbents have been investigated for the fluoride removal, including metal-doped alumina oxide [5], activated carbon [6], bone char [7], synthetic ion exchangers [8], layered double hydroxides [9], and other natural materials [10]. However, there were several problems associated with their use, for example, low adsorption capacity, narrow available pH range and poor selectivity. Thus, much effort has been devoted to develop new fluoride adsorbents with good performance in recent years.

It has been reported that La(III), Ce(IV), Y(III), and Zr(IV) oxides had high adsorption capacity for fluoride [10,11]. Among these adsorbents, zirconium-based materials have been paid more attention in recent investigations due to their high binding affinity with fluoride [12]. In addition, cerium hybrid materials have been also reported as showing good fluoride removal performance as well as having favorable characteristics in terms of cost, environmental impact and chemical stability [13–15]. In order to benefit from the advantages of these two kinds of adsorbents, a combination of cerium and zirconium would be expected to study as a novel adsorbent for the adsorptive removal of fluoride.

In this study, porous CeO_2–ZrO_2 nanocages as a novel type of adsorbent for fluoride removal were prepared. Their uptake capacity and adsorption kinetics for fluoride were investigated.

* Corresponding authors at: Department of Materials Science and Engineering, University of Science and Technology of China, Hefei, Anhui 230026, PR China. Tel.: +86 551 65595607; fax: +86 551 65592420.
E-mail addresses: whxu@iim.ac.cn (W. Xu), xingjiuhuang@iim.ac.cn (X.-J. Huang).

1385-8947/$ - see front matter © 2013 Elsevier B.V. All rights reserved.
http://dx.doi.org/10.1016/j.cej.2013.07.022

The effects of pH, initial fluoride concentration and co-existing anions were examined. Furthermore, the removal mechanism of fluoride was studied by zeta potential measurement, FTIR and XPS analysis. The results suggested that both anion exchange and electrostatic interaction were involved in the adsorption of fluoride.

2. Materials and methods

2.1. Adsorbent preparation

Zirconyl chloride octahydrate ($ZrOCl_2{\cdot}8H_2O$), cerium nitrate hexahydrate ($Ce(NO_3)_3{\cdot}6H_2O$) and ethylene glycol (EG) were obtained from Sinopharm Chemical Reagent Co. (China). All chemicals are of analytical grade, and used in this study without further purification. Milli-Q ultrapure water (18.2 MΩ cm) was used for all the experiments. The synthesis of CeO_2–ZrO_2 nanocages was based on a modified method of that investigated by Liang et al. [16]. Typically, 4 mL 0.5 mol/L $Ce(NO_3)_3$ solution was added in 60 mL EG with stirring, then the mixture was transferred to a sealed Teflon-lined pressure vessel and reacted at 180 °C for 16 h. After the reaction and being cooled down to room temperature, 1.2 mL 0.5 mol/L $ZrOCl_2$ solution was added in the colloid ceria clusters obtained above. Then the mixture was sealed and heated at 180 °C for 8 h. The CeO_2–ZrO_2 nanocages were obtained and washed by ethanol with centrifugated at 10,000 rpm for 6 min several times, and dried under vacuum desiccation oven at 60 °C for 6 h.

2.2. Equipments

The scanning electron microscopy (SEM) images were taken by using a field-emission scanning electron microscopy (SEM, FEI Sirion 200 FEG, operated at 10 kV). X-ray diffraction (XRD) was performed on a D/MaxIIIA X-ray diffractometer, using Cu Kα ($\lambda_{K\alpha1}$ = 1.5418 Å) as the radiation source. The Brunauer–Emmett–Teller (BET) specific surface of CeO_2–ZrO_2 was measured by the nitrogen adsorption and desorption isotherms at 77 K. The Fourier transform infrared (FT-IR) spectra of the obtained samples were recorded with a NEXUS-870 FT-IR spectrometer in the range of 4000–400 cm^{-1}. X-ray photoelectron spectroscopy (XPS) analyses of the samples were conducted on a VG ESCALAB MKII spectrometer using an Mg Kα X-ray source (1253.6 eV, 120 W) at a constant analyzer. The concentration of fluoride was measured using expandable ion analyzer with the fluoride ion selective electrode PF-202-CF (Leici, China) and the study of QA/QC for the fluoride measurement demonstrated that this measurement method is reliable (see Table S1). The concentrations of bicarbonate, chloride, and sulfate anions were measured by ion chromatograph (ICS-2000, USA). The concentration of arsenate in the solution was analyzed using inductively coupled plasma atomic emission spectroscopy (ICP-AES, Thermo Jarrell-Ash Co., USA). The pH was measured with a pH electrode (pH S-3C, China). The zeta potentials of the samples were determined using a zeta potential meter (Zetasizer 2000, Malvern Co., UK).

2.3. Batch adsorption experiments

Before adsorption experiments, standard stock solutions of fluoride (1000 mg/L F) was prepared by dissolving 0.221 g sodium fluoride into 100 mL deionized water from a Milli-Q water system and stored under dark conditions at 4 °C. Fluoride-bearing solutions were prepared by diluting the stock solution to given concentrations with deionized water. And the calibration curve was obtained from the potential of the standard sodium fluoride solutions (0.1–30 mg/L) at pH 4.0 (see the Supplementary material, Fig. S1).

Kinetics experiments were conducted at room temperature. The CeO_2–ZrO_2 nanocages of 0.05 g were immersed in 150 mL fluoride-bearing solutions with the initial fluoride concentrations of 5, 10 and 40 mg/L, respectively. The mixtures were shaken at 140 rpm and approximately 5 mL aliquots were taken from the suspension at predetermined times and quickly separated by centrifugation and 0.22 μm membrane to measure the corresponding fluoride concentration, in order to calculate their time-dependant adsorption capacities.

The adsorption isotherms were studied with a sorbent loading of 0.2 g/L at pH 4.0. Typically, 0.02 g CeO_2–ZrO_2 was added to 100 mL fluoride solutions of varying initial concentrations (1–100 mg/L). The solutions were oscillated at 140 rpm for 24 h to achieve equilibrium, then separated by centrifugation at 10,000 rpm for 3 min, and filtered with a 0.22 μm cellulose membrane. The residual fluoride concentration in solution was measured by the fluoride ion selective electrode PF-202-CF. The adsorption capacity at equilibrium of the adsorbents for fluoride was calculated according to the following equation:

$$q_e = \frac{(C_o - C_e)V}{m} \quad (1)$$

where C_o and C_e represent the initial and equilibrium fluoride concentrations (mg/L) respectively, V is the volume of the fluoride solution (mL), and m is the amount of adsorbent (g).

The effect of pH on the fluoride adsorption was investigated using different initial fluoride concentrations of 10 mg/L, 25 mg/L, and 40 mg/L, respectively, with 0.2 g/L of adsorbent and a total suspension volume of 100 mL. The effects of co-existing anions (bicarbonate, arsenate, chloride, and sulfate) on fluoride adsorption were performed with an adsorbent dose of 0.2 g/L and an initial fluoride concentration of 10 mg/L at pH 4. The co-existing anions were set at five concentration levels of 0, 10, 20, 40 and 50 mg/L, respectively. The mixed suspensions were shaken at 140 rpm for 24 h at room temperature.

3. Results and discussion

3.1. Sorbent characterization

Fig. 1 shows the SEM images of the as-prepared products. It is clear that uniform monodisperse nanocages with an apparent interior void were obtained. The diameter of the obtained nanocages were about 80–100 nm. The hollow nanostructures could be routinely achieved using the Kirkendall effect through the reaction between CeO_2 nanospheres and Zr^{4+} ions. XRD patterns of hollow nanospheres nanocages can be appointed to the face-centered cubic phase (see Fig. S2) [16]. The N_2 adsorption–desorption isotherm and pore size distribution curve implied the presence of multimodal pore structure in the CeO_2–ZrO_2 nanocages (see Fig. S3). The BET surface area of the CeO_2–ZrO_2 hollow nanospheres was investigated to be 29.61 m^2/g.

3.2. Effect of solution pH on fluoride removal

The influence of the pH values on fluoride removal by the CeO_2–ZrO_2 nanocages with various initial concentrations was investigated, and the results are shown in Fig. 2a. It is clear that the optimum pH for the fluoride adsorption was in the range of 3.5–4.5. Thus, the kinetic and isotherm experiments were carried out at pH 4.0 in this study. At pH 4, with initial fluoride concentrations of 10, 25 and 40 mg/L, the equilibrium adsorption capacity were 38.1, 77.5 and 112.7 mg/g, respectively. Furthermore, the adsorption capacities were decreased step by step with the increased pH values, as shown in Fig. 2a, which might be due to the changes

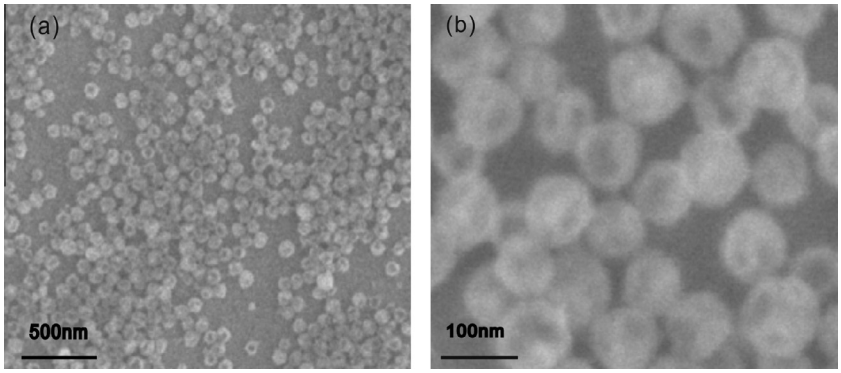

Fig. 1. SEM images of CeO_2–ZrO_2 nanocages at different magnifications.

of pH-dependent electrostatic attraction between the adsorbent surface and fluoride. So, the influence of the pH value on the surface potential was investigated, and the results are shown in Fig. 2b. The CeO_2–ZrO_2 nanocages had a zero point of zeta potential at about pH 7.5, suggesting that the adsorbent surface was positive at pH below 7.5. As a results, the low pH value was favorable for fluoride ions removal owing to the electrostatic attraction. On the contrary, when the pH value was up to and larger than 7.5, the adsorbent surface became negatively charged. The higher pH means the more negative surface, which will result in the strong electrostatic repulsion between adsorbent and the fluoride ions, as well as the clearly decreased adsorption capacities, as shown in Fig. 2a.

In addition, in spite of the increased zeta potential, the adsorption capacities were also decreased with the decrease of pH from 4.0 to 2.0. This might be due to the formation of hydrofluoric acid:

$$H^+\ (aq) + F^-\ (aq) \rightarrow HF\ (aq)$$

which results in lower available fluoride concentration than the actual concentration for adsorption on the adsorbent. It should be mentioned that the adsorption capacities were dramatically decreased and reduced to almost zero when the pH value reached to 10. The results were consistent with the ones of other metal impregnated adsorbents [17,18]. So, the high pH value was benefit to the desorption of fluoride from the adsorbent. We could take this experimental phenomenon as an approach for desorption of fluoride from the adsorbent.

3.3. Kinetic study

The kinetic of adsorption which describes the solute uptake rate governing the residence time of the adsorption reaction is one of the most important characteristics that define the efficiency of adsorption. Fig. 3a depicts the adsorption kinetics of fluoride on the CeO_2–ZrO_2 at various initial concentrations with a sorbent loading of 0.2 g/L at pH 4.0 ± 0.2. It can be found that the adsorption happened rapidly in the first 10 min, and then the adsorption capacity increased gradually till reached the equilibrium. The adsorption equilibrium was achieved within 24 h. Therefore, an optimum shaking time of 24 h was chosen in the subsequent adsorption tests. To further quantify the changes of fluoride adsorption with time on the CeO_2–ZrO_2 nanocages, the pseudo-first-order and pseudo-second-order kinetic models were used to simulate the kinetics. The pseudo-second-order model fits better based on the values of regression coefficients (R^2) (Figs. 3b and S4, Table 1). The equilibrium adsorption capacities (q_e) were calculated as 17.93, 33.13, and 111.6 mg/g when the initial fluoride concentrations were 5, 10, and 40 mg/L, respectively. The value of $q_{e,cal}$ was in agreement with $q_{e,exp}$ based on pseudo-second-order model (Table 1).

In addition, the time-dependent adsorption kinetics studies of the CeO_2–ZrO_2 nanocages were conducted at three different temperatures and analyzed using pseudo-second-order kinetic equations. As shown in Fig. 4 and Table 2, the constant k_2, the initial adsorption rate h_0 and equilibrium adsorption capacity $q_{e,exp}$ values all increased with the increase of temperature from 25 to 55 °C, which suggested that the increase of temperature is beneficial for fluoride adsorption on the adsorbent.

3.4. Adsorption isotherm

To understand the adsorption performance and the adsorption mechanism, adsorption isotherm of fluoride adsorption on the CeO_2–ZrO_2 nanocages were investigated. Fig. 5a shows the

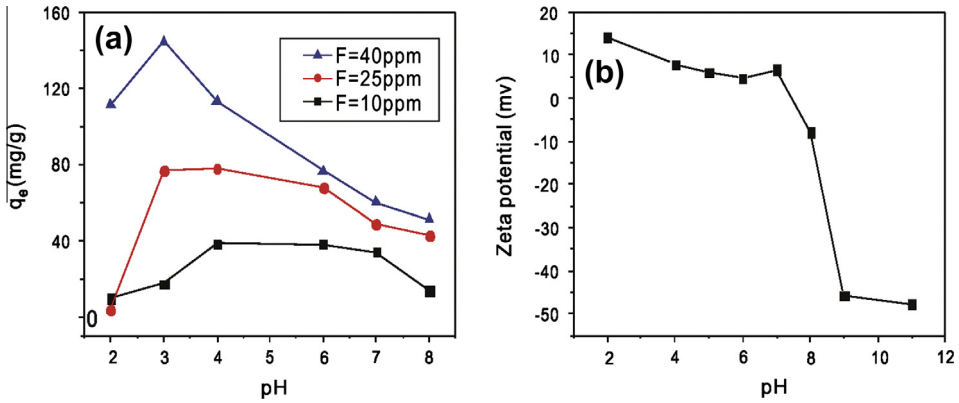

Fig. 2. (a) Effect of pH on the removal of fluoride by CeO_2–ZrO_2 nanocages with initial fluoride concentrations of 10 mg/L, 25 mg/L and 40 mg/L, respectively. (b) Zeta potential of CeO_2–ZrO_2 nanocages as a function of pH. Adsorbent dose: 0.2 g/L, temperature: 25 °C.

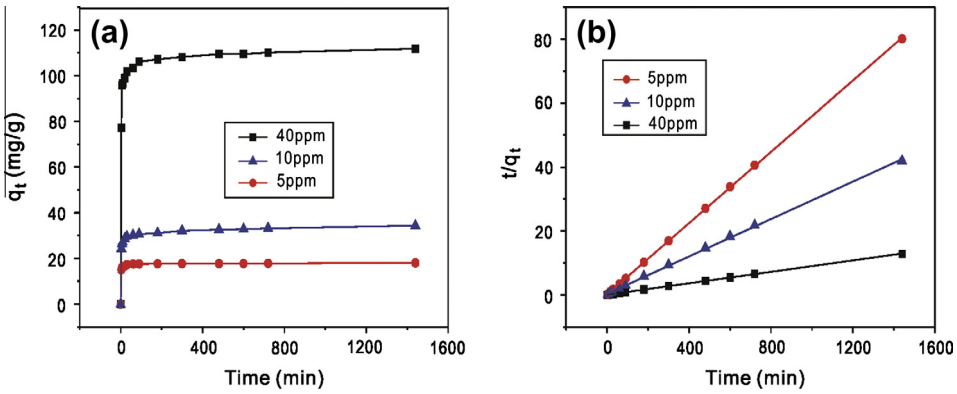

Fig. 3. (a) Adsorption kinetic curves of fluoride adsorption on the CeO_2–ZrO_2 nanocages with different initial fluoride concentration. Adsorbent dose: 0.2 g/L, temperature: 25 °C, pH 4.0 ± 0.2. (b) Pseudo-second-order kinetic plots for the adsorption of fluoride on the CeO_2–ZrO_2 nanocages.

Table 1
Kinetics parameters for flouride adsorption on CeO_2–ZrO_2 nanocages.

Equations		First-order kinetics $\ln(q_e - q_t) = \ln q_e - k_1 t$			Second-order kinetics $\frac{t}{q_t} = \frac{1}{k_2 q_e^2} + \frac{t}{q_e}$		
C_o (mg/L)	$q_{e,exp}$ (mg/g)	k_1 (1/min)	$q_{e,cal}$ (mg/g)	R^2	k_2 (g/(mg min))	$q_{e,cal}$ (mg/g)	R^2
5	17.97	2.8×10^{-3}	1.11	0.554	2.13×10^{-2}	17.93	0.999
10	34.34	2.5×10^{-3}	6.16	0.852	2.93×10^{-3}	33.13	0.999
40	111.85	3.4×10^{-3}	14.36	0.843	1.84×10^{-3}	111.6	0.999

Note: k_1 is the adsorption rate constant for pseudo-first order reaction (1/min). k_2 is the rate constant for pseudo-second order reaction (g/(mg min)). q_e and q_t are the amounts of solute sorbed at equilibrium and at any time t (mg/g), respectively. $q_{e,exp}$ is the adsorption capacity evaluated from batch experiment, while $q_{e,cal}$ is the adsorption capacity calculated on the basis of the pseudo-first-order and pseudo-second-order equations.

adsorption isotherms at pH 4.0 ± 0.2. Both Freundlich and Langmuir models were applied to describe the experimental adsorption results (Figs. 5b and S5, Table 3) [19,20].

Figs. 5b and S5, Table 3 show that the Langmuir model gave a better fit to the experimental data than Freundlich isotherm based on the R^2 values. The maximum adsorption capacity of CeO_2–ZrO_2 calculated from the linear form of Langmuir model was 175 mg/g (inset of Fig. 5b). To the best of our knowledge, the as-prepared CeO_2–ZrO_2 nanocages had a much higher adsorption capacity than that of the other adsorbents reported previously (Table 4). The BET surface area of the CeO_2–ZrO_2 nanocages was not higher than other adsorbents, but had a much higher adsorption capacity (Table 4), suggesting that the surface area might not be the dominant factor in the fluoride adsorption [18]. The abundant surface hydroxyl groups on CeO_2–ZrO_2 nanocages and pH effect might be attributed to the excellent fluoride removal. The superior adsorption capacity of the CeO_2–ZrO_2 nanocages for fluoride indicates that it could be a potential candidate for water treatment in future practical application.

3.5. Effect of co-existing ions

Taking the complexity of water source into account, more than one anion might be present such as sulfate, chloride, bicarbonate and arsenate. Considering the competition for the binding sites between fluoride ions and these anions, they might interfere with the removal efficiency of fluoride. So, the effect of various co-existing ions upon adsorption of fluoride was investigated, and the results are shown in Fig. 6. The results indicated that sulfate had little effect upon fluoride removal when their concentrations were equal or multiples of the concentration of fluoride. The presence of HCO_3^- significantly affected the fluoride removal. HCO_3^- ion is

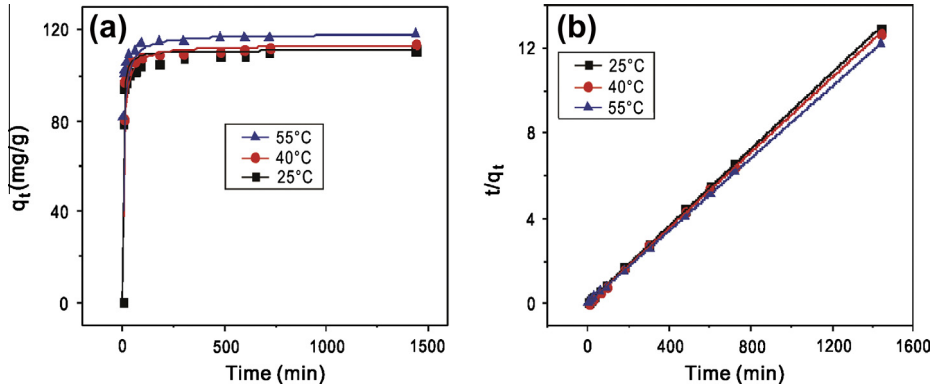

Fig. 4. (a) Adsorption kinetics of fluoride removal by the CeO_2–ZrO_2 nanocages at different temperatures. (b) Pseudo-second order model for fluoride removal by the CeO_2–ZrO_2 nanocages at different temperatures. Adsorbent dose: 0.2 g/L, pH 4.0 ± 0.2.

Table 2
Fluoride adsorption pseudo-second-order kinetic constants for CeO_2–ZrO_2 nanocages at different temperatures with initial fluoride concentration of 40 mg/L.

Initial temp. (°C)	$q_{e,exp}$ (mg/g)	h_0 (mg/(g min))	k_2 (g/(mg min))	$q_{e,cal}$ (mg/g)	R^2
25	111.19	22.85	1.86×10^{-3}	110.99	0.9998
40	113.51	27.81	2.17×10^{-3}	113.25	0.9998
55	118.18	34.29	2.46×10^{-3}	117.92	0.9999

Note: The initial sorption rate, h_0 (mg/(g min)) can be defined as: $h_0 = k_2 q_e^2 \quad (t \to 0)$.

Table 3
Langmuir and Freundlich adsorption isotherm parameters for fluoride on CeO_2–ZrO_2 nanocages.

Equations	Langmuir model $\frac{C_e}{q_e} = \frac{C_e}{q_m} + \frac{1}{q_m k_L}$			Freundlich model $\ln q_e = \frac{1}{n}\ln C_e + \ln k$		
Parameters	K_L (L/mg)	q_m (mg/g)	R^2	n	k	R^2
Values	0.075	175	0.994	1.44	12.60	0.939

Note: C_e is the equilibrium concentration of fluoride (mg/L); q_e is the amount of fluoride adsorbed on per weight of adsorbent after equilibrium (mg/g); q_m represents the maximum adsorption capacity of fluoride on per weight of adsorbent (mg/g); k_L is the Langmuir constant related to the energy of adsorption (L/mg); q_m and k_L were calculated from the slope and intercept of the linear plots of C_e/q_e vs C_e. The Freundlich constant k is correlated to the relative adsorption capacity of the adsorbent (mg/g), and $1/n$ is the adsorption intensity.

hydrolyzed in solution, leading to the increase of pH value (Fig. S6). As a result, more hydroxyl ions would compete with fluoride on the active adsorption sites [14], which resulted in the decrease of adsorption capacity of the CeO_2–ZrO_2 nanocages for fluoride. This result was in agreement with the effect of pH discussed above. In addition, chloride and arsenate only showed some adverse effects on fluoride adsorption at high concentrations.

3.6. Removal of fluoride from real sample

To examine the fluoride removal performance by the CeO_2–ZrO_2 nanocages in the natural water environment, fluoride adsorption studies of the adsorbent on an underground water sample from Inner Mongolia of China were conducted. Table 5 displays the characteristics of the underground water sample, demonstrating the complexity of substances in the water and high fluoride concentration exceeding the limit of safe drinking. Fig. 7 shows the effect of adsorbent dose on the fluoride removal of the water sample after 60-min treatment. The residual fluoride concentration decreased with the increase in adsorbent dose. At an adsorbent dose of 0.4 g/L, the fluoride concentration in the water sample was reduced from 2.82 mg/L to about 1.39 mg/L after the treatment, which meets the guideline limit of fluoride in drinking water regulated by the WHO (1.5 mg/L). This application implies that the adsorbent could be potentially used in practical drinking water treatment.

Furthermore, in order to evaluate the practical defluoridation capacity of the CeO_2–ZrO_2 nanocages in different natural water environments, several underground water samples with different fluoride concentrations were collected from different locations in Inner Mongolia of China. The water characteristics of Sample 2 are shown in Table 5, others can be found in Table S2. The fluoride concentrations of Samples 1–4 were 3.29, 2.82, 2.35, and 2.00 mg/L, respectively. Additionally, it is necessary to investigate the removal performance of the adsorbent in high fluoride contaminated waters. We added the standard stock solutions of fluoride into Samples 1–4 to make new Samples 1*–4* with fluoride concentrations of 13.09, 12.70, 12.30, and 11.92 mg/L, respectively. The kinetics studies of fluoride adsorption by the adsorbent on these water samples are shown in Fig. 8. The experimental results demonstrated that the water samples with a higher fluoride concentration needed a high adsorbent dose to remove fluoride to the guideline limit regulated by the WHO. The fluoride concentration of 3.29 mg/L could be decreased to below 1.5 mg/L at pH 7 within 60 min using adsorbent dose of 1 g/L, while the fluoride concentration of 13.09 mg/L needed an adsorbent dose of 2 g/L. The reason

Table 4
Comparison of adsorption capacity with different adsorbents and the corresponding parameters.

Adsorbent	Adsorption capacity (mg/g)	BET (m^2/g)	pH	References
Hydrous zirconium oxide	124	n.a.	4	[12]
Zirconium oxide	19	n.a.	4.75	[21]
$ZrO_2/SiO_2/Fe_3O_4$	14.7	4.6	4.0	[22]
Fe–Al–Ce trimetal oxide	178	90	7.0	[18]
CTAB assisted mixed iron oxide	40.4	201.9	5.0	[23]
Hydrous ferric oxide	16.5	n.a.	5.0	[24]
Nano-sized goethite (α-FeOOH)	59	n.a.	5.75	[25]
Zirconium-modified-Na-attapulgite	24.55	n.a.	4.13	[26]
CeO_2–ZrO_2 nanocages	175	29.61	4	Present work

n.a. = not available.

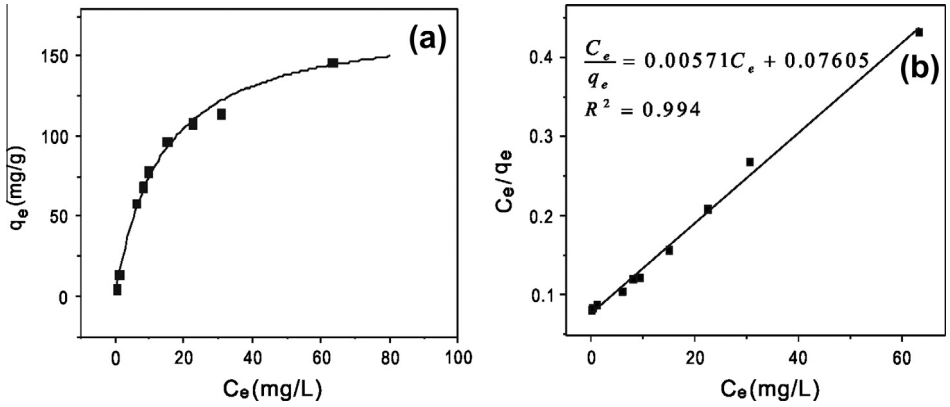

Fig. 5. (a) Adsorption isotherms of fluoride on CeO_2–ZrO_2 nanocages. Adsorbent dose: 0.2 g/L, temperature: 25 °C, pH 4.0 ± 0.2. (b) Langmuir isotherm models for fitting of fluoride adsorption on CeO_2–ZrO_2 nanocages. Inset is the linear form of Langmuir model equation.

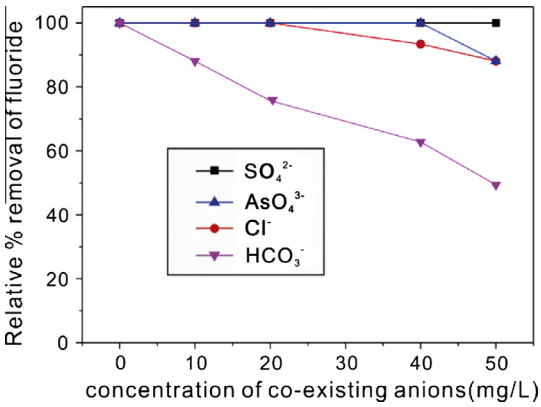

Fig. 6. Effects of co-existing anions on fluoride removal by CeO_2–ZrO_2 nanocages at pH 4. Adsorbent dose: 0.2 g/L, Initial fluoride concentration: 10 mg/L, temperature: 25 °C.

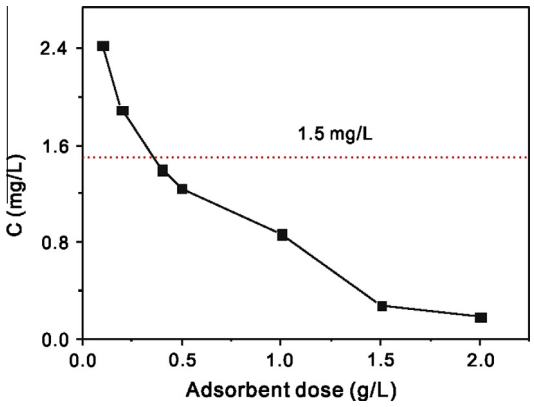

Fig. 7. Effect of adsorbent dose on fluoride removal of the water sample from Xingwang Village in Inner Mongolia. Temperature: 25 °C, pH 7.0 ± 0.2, treatment time: 60 min.

Table 5
Characteristics of the natural water sample from Xingwang Village in Inner Mongolia of China.

Items	Value
Fluoride (mg/L)	2.820
Chloride (mg/L)	119.6
As (mg/L)	0.103
Sulfate (mg/L)	4.740
Hg (mg/L)	0.006
Pb (mg/L)	0.003

might be the complex competing effect from other species in natural water and pH effect. However, it is important to mention that the fluoride concentration of 13.09 mg/L could be easily reduced to below 1.5 mg/L with only a low adsorbent dose of 0.4 g/L at pH 4 (Fig. S8).

3.7. Mechanism of fluoride adsorption

Revealing the adsorption mechanism plays an important role in understanding the material characteristics and designing the application purpose of the new adsorbent. It has been reported the hydrolysis reaction occurring between the metal oxide and water results in the formation of surface hydroxyl groups. The surface hydroxyl groups on metal oxides are considered as the most abundant and active adsorption sites for adsorption of anions from water [11,27]. So, CeO_2–ZrO_2 nanocages before and after fluoride adsorption were characterized by FTIR, and the results are shown in Fig. 9.

From the IR spectrum of before adsorption, the peak at 1358 cm^{-1} was assigned to the bending vibration of Zr–OH groups [12]. It could be seen that after adsorption, the peak at 1358 cm^{-1} disappeared. This confirms that fluoride has replaced a substantial fraction of surface hydroxyl groups bound to zirconium. It is interesting that the new peaks at 581 and 1433 cm^{-1} appeared in the spectrum of the fluoride-sorbed adsorbent, which may be due to the M–F bonds formed after fluoride adsorption (M = Ce or Zr) [14,28]. When the adsorbent was calcined at 800 °C, the peak at 1358 cm^{-1} almost disappeared, which means only few of surface hydroxyl groups existing after calcination. Furthermore, the adsorption properties of the calcined adsorbent was also investigated, and the results suggested that the adsorption properties decreased step by step with the increased calcination temperature (see Fig. S7). So, the results further verified the important roles of surface hydroxyl group in the adsorption of fluoride.

To further investigate the roles of the surface hydroxyl group, CeO_2–ZrO_2 adsorbent before and after fluoride adsorption were further characterized by XPS, and the results are shown in Fig. 10. From Fig. 10a, the strong peaks at 685 eV was assigned to the F_{1s} photoelectron, indicating that F was effectively taken up by the adsorbent.

The O 1s spectrum was divided into three peaks, that are metal oxide (M–O), hydroxyl bonded to metal (M–OH) and adsorbed

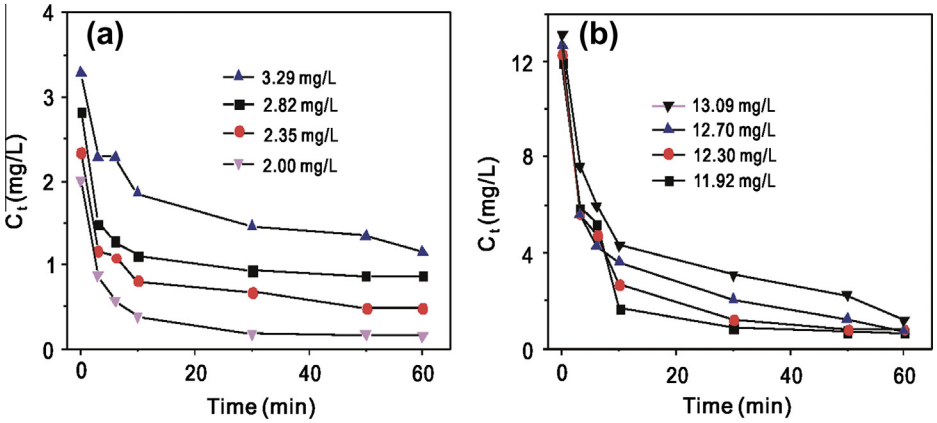

Fig. 8. Kinetics adsorption experiment on (a) water Samples 1–4 with adsorbent dose of 1.0 g/L and (b) water Samples 1*–4* with adsorbent dose of 2.0 g/L at pH 7, temperature: 25 °C.

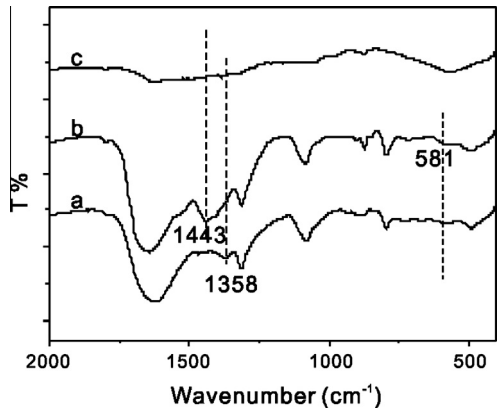

Fig. 9. FTIR spectra of the CeO_2–ZrO_2 nanocages before adsorption (a) and after (b) fluoride adsorption at 40 mg/L, as well as (c) the CeO_2–ZrO_2 adsorbent calcined at 800 °C.

water (H_2O), respectively [29], as shown in Fig. 10c–d and Table 6. Surface hydroxyl, which was proven to be the key factor for F adsorption by CeO_2–ZrO_2, occupied 64.09% in CeO_2–ZrO_2 (Table 6). After fluoride adsorption, the content of the surface hydroxyl groups decreased from the 64.09% to 51.56%, which further confirmed the important roles of the surface hydroxyl groups in the adsorption of fluoride, which was consistent with result of FTIR analysis.

Table 6
O(1s) peak parameters for before and after fluoride adsorption on CeO_2–ZrO_2 nanocages.

Sample	Peak[a]	B.E. (eV)	Percent (%)[b]
CeO_2–ZrO_2	O^{2-}	528.87	4.13
	M–OH	531.07	64.09
	H_2O	531.89	31.78
CeO_2–ZrO_2–F	O^{2-}	529.08	14.87
	M–OH	531.27	51.56
	H_2O	531.92	33.57

[a] Surface species: O^{2-}: oxygen bonded to metal; OH^-: hydroxyl bonded to metal; H_2O: sorbed water.
[b] The percentage represents the contribution of each peak to the total number of counts under the O(1s) peak. M = Ce or Zr.

4. Conclusions

This study demonstrates that the porous CeO_2–ZrO_2 nanocages showed excellent fluoride removal performance. The adsorption isotherm could be described very well by the Langmuir model, and the maximum capacity was calculated to be 175 mg/g at pH 4.0, which was much higher than that of other adsorbents previously reported. Co-existence of chloride and arsenate only showed some adverse effects on fluoride adsorption in high concentrations. The presence of sulfate has no influence on the fluoride adsorption. On the contrary, HCO_3^- obviously reduced the removal efficiency owing to its hydrolysis. The adsorption mechanism of the

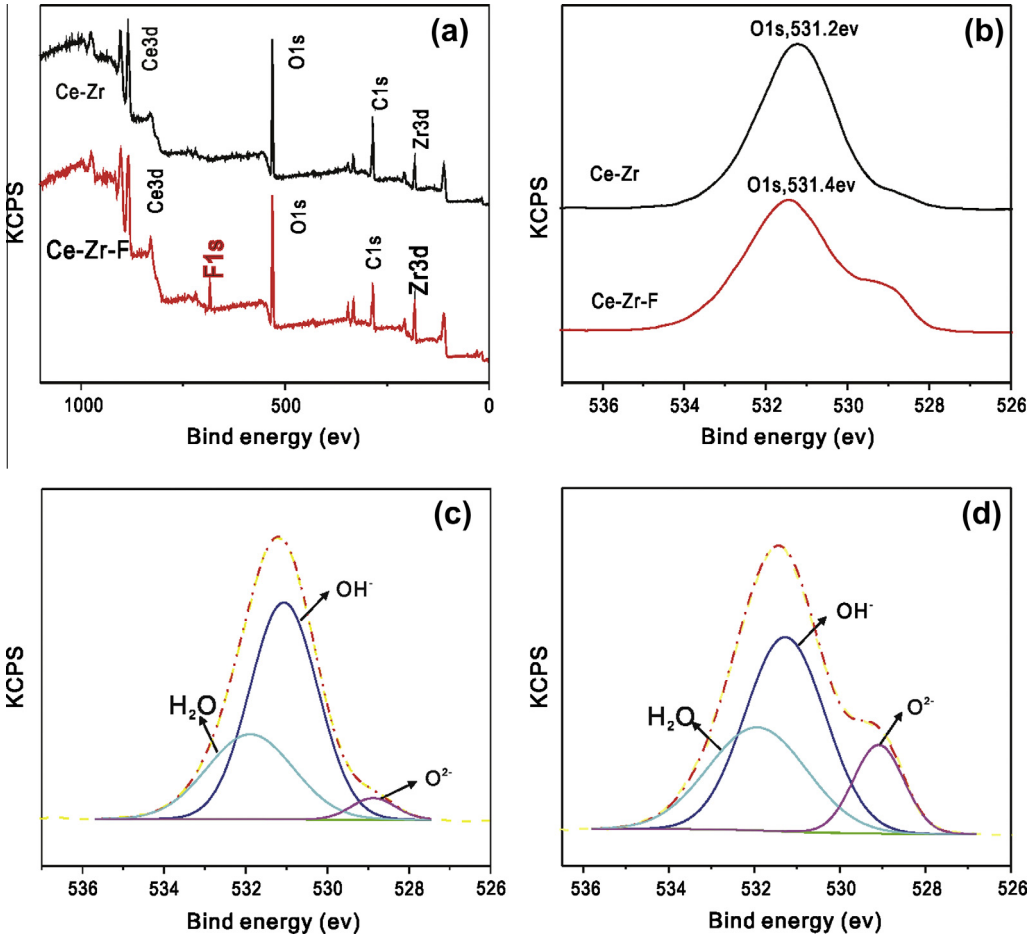

Fig. 10. XPS spectra of (a) CeO_2–ZrO_2 and (b) O 1s, before and after adsorption; O 1s spectra of (c) CeO_2–ZrO_2 and (d) CeO_2–ZrO_2 after F adsorption. The peak at the lowest binding energy is oxide (O^{2-}), the peak with intermediate binding energy is M–OH, and the highest energy peak is that of H_2O.

adsorbent for fluoride could involve anion exchange and electrostatic interaction based on zeta potential measurement, FTIR and XPS. This research results indicated that the as-prepared CeO_2–ZrO_2 adsorbent could be a potentially suitable material used in the fluoride removal. In the future, industrial-grade raw materials will replace analytical-grade chemicals to synthesize the adsorbent. Additionally, in order to better apply the CeO_2–ZrO_2 hollow nanospheres for practical water application in the future, we are planning to use a sol–gel method to embed the adsorbent in a chitosan matrix to further reduce the cost of the adsorbents and their application.

Acknowledgements

This work was supported by the National Basic Research Program of China (2011CB933700), the Natural Science Foundation of China (50901073 and 90923033), and the One Hundred Person Project of the Chinese Academy of Sciences, China.

Appendix A. Supplementary material

Supplementary data associated with this article can be found, in the online version, at http://dx.doi.org/10.1016/j.cej.2013.07.022.

References

[1] E.J. Reardon, Y.X. Wang, A limestone reactor for fluoride removal from wastewaters, Environ. Sci. Technol. 34 (2000) 3247–3253.
[2] F. Shen, X.M. Chen, P. Gao, G.H. Chen, Electrochemical removal of fluoride ions from industrial wastewater, Chem. Eng. Sci. 58 (2003) 987–993.
[3] WHO, Guidelines for drinking water quality, 1, 2nd ed., Geneva, 1993.
[4] X.P. Liao, B. Shi, Adsorption of fluoride on zirconium (IV)-impregnated collagen fiber, Environ. Sci. Technol. 39 (2005) 4628–4632.
[5] S.S. Tripathy, A.M. Raichur, Abatement of fluoride from water using manganese dioxide-coated activated alumina, J. Hazard. Mater. 153 (2008) 1043–1051.
[6] A.A.M. Daifullah, S.M. Yakout, S.A. Elreefy, Adsorption of fluoride in aqueous solutions using $KMnO_4$-modified activated carbon derived from steam pyrolysis of rice straw, J. Hazard. Mater. 147 (2007) 633–643.
[7] N.A. Medellin-Castillo, R. Leyva-Ramos, R. Ocampo-Perez, R.F.G. de la Cruz, A. Aragon-Pina, J.M. Martinez-Rosales, R.M. Guerrero-Coronado, L. Fuentes-Rubio, Adsorption of fluoride from water solution on bone char, Ind. Eng. Chem. Res. 46 (2007) 9205–9212.
[8] N. Viswanathan, S. Meenakshi, Role of metal ion incorporation in ion exchange resin on the selectivity of fluoride, J. Hazard. Mater. 162 (2009) 920–930.
[9] L. Lv, J. He, M. Wei, D.G. Evans, Z.L. Zhou, Treatment of high fluoride concentration water by MgAl–CO_3 layered double hydroxides: kinetic and equilibrium studies, Water Res. 41 (2007) 1534–1542.
[10] S. Meenakshi, C.S. Sundaram, R. Sukumar, Enhanced fluoride sorption by mechanochemically activated kaolinites, J. Hazard. Mater. 153 (2008) 164–172.
[11] S. Tokunaga, M.J. Haron, S.A. Wasay, K.F. Wong, K. Laosangthum, A. Uchiumi, Removal of fluoride ions from aqueous solutions by multivalent metal compounds, Int. J. Environ. Studies 48 (1995) 17–28.
[12] X.M. Dou, D. Mohan, C.U. Pittman, S. Yang, Remediating fluoride from water using hydrous zirconium oxide, Chem. Eng. J. 198 (2012) 236–245.
[13] L. Chen, T.-J. Wang, H.-X. Wu, Y. Jin, Y. Zhang, X.-M. Dou, Optimization of a Fe–Al–Ce nano-adsorbent granulation process that used spray coating in a fluidized bed for fluoride removal from drinking water, Powder Technol. 206 (2011) 291–296.
[14] H. Liu, S.B. Deng, Z.J. Li, G. Yu, J. Huang, Preparation of Al–Ce hybrid adsorbent and its application for defluoridation of drinking water, J. Hazard. Mater. 179 (2010) 424–430.
[15] X.M. Dou, Y.S. Zhang, H.J. Wang, T.J. Wang, Y.L. Wang, Performance of granular zirconium–iron oxide in the removal of fluoride from drinking water, Water Res. 45 (2011) 3571–3578.
[16] X. Liang, X. Wang, Y. Zhuang, B. Xu, S.M. Kuang, Y.D. Li, Formation of CeO_2–ZrO_2 solid solution nanocages with controllable structures via Kirkendall effect, J. Am. Chem. Soc. 130 (2008) 2736–2737.
[17] X.L. Zhao, J.M. Wang, F.C. Wu, T. Wang, Y.Q. Cai, Y.L. Shi, G.B. Jiang, Removal of fluoride from aqueous media by Fe_3O_4@$Al(OH)_3$ magnetic nanoparticles, J. Hazard. Mater. 173 (2010) 102–109.
[18] X. Wu, Y. Zhang, X. Dou, M. Yang, Fluoride removal performance of a novel Fe–Al–Ce trimetal oxide adsorbent, Chemosphere 69 (2007) 1758–1764.
[19] I. Langmuir, The constitution and fundamental properties of solids and liquids, J. Am. Chem. Soc. 38 (1916) 2221–2295.
[20] H.M.F. Freundlich, Über die adsorption in ösungen, Z. Phys. Chem. 57 (1906) 385–470.
[21] J.A. Blackwell, P.W. Carr, Study of the Fluoride adsorption characteristics of porous microparticulate zirconium-oxide, J. Chromatogr. 549 (1991) 43–57.
[22] C.F. Chang, C.Y. Chang, T.L. Hsu, Removal of fluoride from aqueous solution with the superparamagnetic zirconia material, Desalination 279 (2011) 375–382.
[23] M. Mohapatra, K. Rout, P. Singh, S. Anand, S. Layek, H.C. Verma, B.K. Mishra, Fluoride adsorption studies on mixed-phase nanoiron oxides prepared by surfactant mediation–precipitation technique, J. Hazard. Mater. 186 (2011) 1751–1757.
[24] S.G. Soumen Dey, Uday Chand Ghosh, Hydrous ferric oxide (HFO) – a scavenger for fluoride from contaminated water, Water Air Soil Pollut. 158 (2004) 311–323.
[25] M. Mohapatra, K. Rout, S.K. Gupta, P. Singh, S. Anand, B.K. Mishra, Facile synthesis of additive-assisted nanogoethite powder and its application for fluoride remediation, J. Nanopart. Res. 12 (2010) 681–686.
[26] G. Zhang, Z.L. He, W. Xu, A low-cost and high efficient zirconium-modified-Na-attapulgite adsorbent for fluoride removal from aqueous solutions, Chem. Eng. J. 183 (2012) 315–324.
[27] H. Tamura, K. Mita, A. Tanaka, M. Ito, Mechanism of hydroxylation of metal oxide surfaces, J. Colloid Interface Sci. 243 (2001) 202–207.
[28] W.S. Dong, F.Q. Lin, C.L. Liu, M.Y. Li, Synthesis of ZrO_2 nanowires by ionic-liquid route, J. Colloid Interface Sci. 333 (2009) 734–740.
[29] S.B. Deng, H. Liu, W. Zhou, J. Huang, G. Yu, Mn–Ce oxide as a high-capacity adsorbent for fluoride removal from water, J. Hazard. Mater. 186 (2011) 1360–1366.